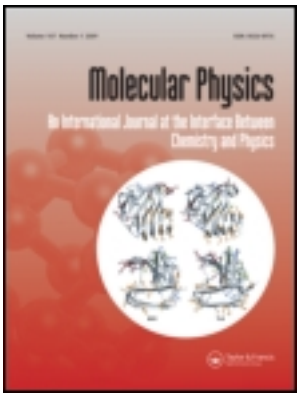

Molecular Physics: An International Journal at the Interface Between Chemistry and Physics

Publication details, including instructions for authors and subscription information:
http://www.tandfonline.com/loi/tmph20

Cross-polarization dynamic-angle spinning nuclear magnetic resonance of quadrupolar nuclei

Jay H. Baltisberger [a b d], Sheryl L. Gann [a d], Philip J. Grandinetti [a c d] & Alexander Pines [a d]

[a] Materials Sciences Division, Lawrence Berkeley Laboratory, Berkeley, CA, 94720, USA

[b] Department of Chemistry, Berea College, Berea, KY, 40404, USA

[c] Department of Chemistry, Ohio State University, Columbus, OH, 43210, USA

[d] University of California, Berkeley, CA, 94720, USA

Version of record first published: 26 Oct 2007.

To cite this article: Jay H. Baltisberger , Sheryl L. Gann , Philip J. Grandinetti & Alexander Pines (1994): Cross-polarization dynamic-angle spinning nuclear magnetic resonance of quadrupolar nuclei, Molecular Physics: An International Journal at the Interface Between Chemistry and Physics, 81:5, 1109-1124

To link to this article: http://dx.doi.org/10.1080/00268979400100741

MOLECULAR PHYSICS, 1994, VOL. 81, No. 5, 1109–1124

Cross-polarization dynamic-angle spinning nuclear magnetic resonance of quadrupolar nuclei

by JAY H. BALTISBERGER†, SHERYL L. GANN, PHILIP J. GRANDINETTI‡ and ALEXANDER PINES §

Materials Sciences Division, Lawrence Berkeley Laboratory, and University of California, Berkeley, CA 94720, USA

(*Received 11 October 1993; accepted 13 October 1993*)

The use of variable-angle spinning (VAS) with cross-polarization (CP) for quadrupolar nuclei has been evaluated both experimentally and theoretically. It is known that under normal spinning speeds the best VAS angle for performing CP is 0° (parallel to the magnetic field). We show that, with the use of dynamic-angle spinning (DAS) probes, CP may be done at 0° and detection in a one-dimensional VAS experiment may be performed at any angle in a zero-polarized VAS (ZPVAS) experiment. Finally, the combination of CP with $k = 5$ DAS (where the sample is spun first at 0° followed by 63·43°) provides both the highest resolution and the greatest sensitivity under normal conditions.

1. Introduction

Significant increases in nuclear magnetic resonance (NMR) sensitivity can be achieved by transferring high nuclear spin polarization between inequivalent nuclei using cross-polarization (CP) techniques [1]. In addition, selective CP transfer can be applied as a useful tool for spectral editing [2–9]. While CP is very effective technique for static samples, the combination of CP with high-resolution solid-state NMR techniques that require sample rotation suffers from a number of difficulties. One of these difficulties is that the dipolar spin interactions that mediate the CP transfer become time dependent under magic-angle spinning (MAS), making the Hartmann–Hahn matching conditions more complicated and also reducing the efficiency of the polarization transfer [10]. Another difficulty arises when cross-polarizing the central transition of half-integer quadrupolar nuclei. In this situation, the time dependence of the large first-order quadrupolar interaction interferes with the Hartmann–Hahn matching [11, 12].

Dynamic-angle spinning (DAS) NMR provides high-resolution isotropic spectra for the central transition of half-integer quadrupolar nuclei, which are broadened owing to second-order effects, by making the angle of the spinner axis a time-dependent variable [13–15]. This additional degree of freedom not only gives high-resolution spectra but, as we have shown previously [16–18], provides a solution to the problem of combining CP with high-resolution solid-state NMR techniques. This solution exploits the time independence of the spin eigenvalues when spinning at 0°

† Present address: Department of Chemistry, Berea College, Berea, KY 40404, USA.
‡ Present address: Department of Chemistry, Ohio State University, Columbus, OH 43210, USA.
§ Author for correspondence.

(parallel) with respect to the external magnetic field. By performing CP while spinning at 0°, the full static CP intensity can be obtained and used in a MAS, variable-angle spinning (VAS) or DAS experiment. A similar technique has been used by Fyfe *et al.* [19,20] to improve CP transfer between the central transition of half-integer quadrupolar nuclei and spin-$\frac{1}{2}$ nuclei such as ^{31}P and ^{29}Si, which often have inefficient relaxation mechanisms.

In this paper, we summarize the basic theory of CP of the central transition in a rotating solid and discuss experimental examples of CP under various sample rotation conditions.

2. Theoretical analysis

The theory of spin locking and CP of the central transition of half-odd integer nuclei has been described in detail by Vega [11,12]. In this section, for completeness, we present a condensed treatment of this problem.

In the CP experiment involving polarization transfer from a spin $I = \frac{1}{2}$ to the central transition of a quadrupolar spin $S = \frac{3}{2}$, the observable of interest, $\langle S_+(t)\rangle$, is obtained from the relation

$$\langle S_+(t)\rangle = \mathrm{Tr}\,[\sigma(t)S_+]. \tag{1}$$

Here, $\sigma(t)$ is the density operator whose evolution is given by

$$\sigma(t) = U(t)\sigma(0)U^\dagger(t), \tag{2}$$

where

$$U(t) = T\exp\left(-\mathrm{i}\int_0^t H(s)\,\mathrm{d}s\right), \tag{3}$$

T is the time-ordering operator and $H(t)$ is the Hamiltonian. The secular Hamiltonian in the rotating frame is given by

$$H(t) = H_{\mathrm{RF}} + H_{\mathrm{D}}(t) + H_{\mathrm{Q}}(t), \tag{4}$$

where

$$H_{\mathrm{RF}} = -\omega_{1I}I_x - \omega_{1S}S_x, \tag{5}$$

$$H_{\mathrm{D}}(t) = \omega_{\mathrm{D}}A_{20}^{\mathrm{D}}(t)2I_zS_z, \tag{6}$$

$$H_{\mathrm{Q}}(t) = \omega_{\mathrm{Q}}A_{20}^{\mathrm{Q}}(t)\tfrac{1}{2}[3S_z^2 - S(S+1)], \tag{7}$$

ω_{1I} and ω_{1S} are the r.f. field strengths, and $A_{20}^{\mathrm{D}}(t)$ and $A_{20}^{\mathrm{Q}}(t)$ are irreducible spherical tensors with principal axis system (PAS) elements $\rho_{20} = 1$ and $\rho_{2\pm2} = \eta/6^{1/2}$ ($\eta = 0$ for the dipolar interaction). The heteronuclear dipolar coupling between two spins, $I = \frac{1}{2}$ and $S = \frac{3}{2}$, and the quadrupolar coupling constant of the $S = \frac{3}{2}$ spin are given by $\omega_{\mathrm{D}} = \mu_0\gamma_I\gamma_S\hbar^2/4\pi r^3$ and $\omega_{\mathrm{Q}} = 3e^2qQ/\hbar 2S(2S-1)$ respectively. It is convenient to rewrite this Hamiltonian in the fictitious spin-$\frac{1}{2}$ formalism [21, 22] (see appendix) as

$$\begin{aligned} H(t) = {} & -\omega_{1I}I_x - 3^{1/2}\omega_{1S}(S_x^{1-2} + S_x^{3-4}) - 2\omega_{1S}S_x^{2-3} + \omega_{\mathrm{Q}}A_{20}^{\mathrm{Q}}(t)(S_z^{1-2} - S_z^{3-4}) \\ & + 3\omega_{\mathrm{D}}A_{20}^{\mathrm{D}}(t)2I_zS_z^{1-4} + \omega_{\mathrm{D}}A_{20}^{\mathrm{D}}(t)2I_zS_z^{2-3}. \end{aligned} \tag{8}$$

We assume that $|\omega_{1I}|$, $|\omega_{1S}| \gg |\omega_{\mathrm{D}}|$ and transform into a time-dependent frame [23]

that diagonalizes $H_{RF} + H_Q(t)$ using

$$W(t) = \exp(-\tfrac{1}{2}i\pi I_y) \exp(\tfrac{1}{2}i\pi S_y^{1-4}) \exp(-\tfrac{1}{2}i\pi S_y^{2-3}) \exp[i2\xi_1(t)S_y^{1-3}] \exp[i2\xi_2(t)S_y^{2-4}], \tag{9}$$

where

$$\tan[2\xi_1(t)] = \frac{3^{1/2}\omega_{1S}}{-\omega_Q A_{20}^Q(t) + \omega_{1S}} \tag{10}$$

and

$$\tan[2\xi_2(t)] = \frac{3^{1/2}\omega_{1S}}{-\omega_Q A_{20}^Q(t) - \omega_{1S}}. \tag{11}$$

The propagator in this time-dependent frame is given by

$$\tilde{U}(t) = T \exp\left(-i\int_0^t [\tilde{H}(s) - i\dot{W}^\dagger(s)W(s)]\,ds\right), \tag{12}$$

where

$$\begin{aligned}\tilde{H}(t) &= W^\dagger(t)H(t)W(t)\\ &= -\omega_{1I}I_z + \omega_{1S}(S_z^{1-4} - S_z^{2-3}) - \omega^{1-3}(t)S_z^{1-3} - \omega^{2-4}(t)S_z^{2-4}\\ &\quad - b_{IS}^{1-4}(t)2I_xS_x^{1-4} - b_{IS}^{2-3}(t)2I_xS_x^{2-3} - b_{IS}^{1-2}(t)2I_xS_x^{1-2} - b_{IS}^{3-4}(t)2I_xS_x^{3-4}\end{aligned} \tag{13}$$

with

$$\omega^{1-3}(t) = \{3\omega_{1S}^2 + [\omega_Q A_{20}^Q(t) - \omega_{1S}]^2\}^{1/2} = \frac{-\omega_Q A_{20}^Q(t) + \omega_{1S}}{\cos[2\xi_1(t)]}, \tag{14}$$

$$\omega^{2-4}(t) = -\{3\omega_{1S}^2 + [\omega_Q A_{20}^Q(t) + \omega_{1S}]^2\}^{1/2} = \frac{\omega_Q A_{20}^Q(t) + \omega_{1S}}{\cos[2\xi_2(t)]}, \tag{15}$$

$$b_{IS}^{1-4}(t) = \omega_D A_{20}^D(t)\{2\cos[\xi_1(t) - \xi_2(t)] + \cos[\xi_1(t) + \xi_2(t)]\}, \tag{16}$$

$$b_{IS}^{1-2}(t) = \omega_D A_{20}^D(t)\{2\sin[\xi_1(t) - \xi_2(t)] - \sin[\xi_1(t) + \xi_2(t)]\}, \tag{17}$$

$$b_{IS}^{2-3}(t) = \omega_D A_{20}^D(t)\{2\cos[\xi_1(t) - \xi_2(t)] - \cos[\xi_1(t) + \xi_2(t)]\}, \tag{18}$$

$$b_{IS}^{3-4}(t) = \omega_D A_{20}^D(t)\{2\sin[\xi_1(t) - \xi_2(t)] + \sin[\xi_1(t) + \xi_2(t)]\} \tag{19}$$

and

$$i\dot{W}^\dagger(t)W(t) = 2\frac{d\xi_1(t)}{dt}S_y^{1-3} + 2\frac{d\xi_2(t)}{dt}S_y^{2-4}, \tag{20}$$

where $0 \leqslant \{\xi_1(t), \xi_2(t)\} \leqslant \frac{1}{2}\pi$. Since $\tilde{U}(t)$ is related to the rotating-frame propagator by $U(t) = W(t)\tilde{U}(t)W^\dagger(0)$, equation (1) can be rewritten

$$\langle S_+(t)\rangle = \mathrm{Tr}[\tilde{U}(t)\tilde{\sigma}(0)\tilde{U}^\dagger(t)\tilde{S}_+], \tag{21}$$

where $\tilde{S}_+ = W^\dagger(t)S_+W(t)$ and $\tilde{\sigma}(0) = W^\dagger(0)\sigma(0)W(0)$. After an initial $\frac{1}{2}\pi$ pulse on the I spin, the initial density operator is $\sigma(0) = I_x$, and the transformed initial density operator is

$$\tilde{\sigma}(0) = W^\dagger(0)\sigma(0)W(0) = I_z. \tag{22}$$

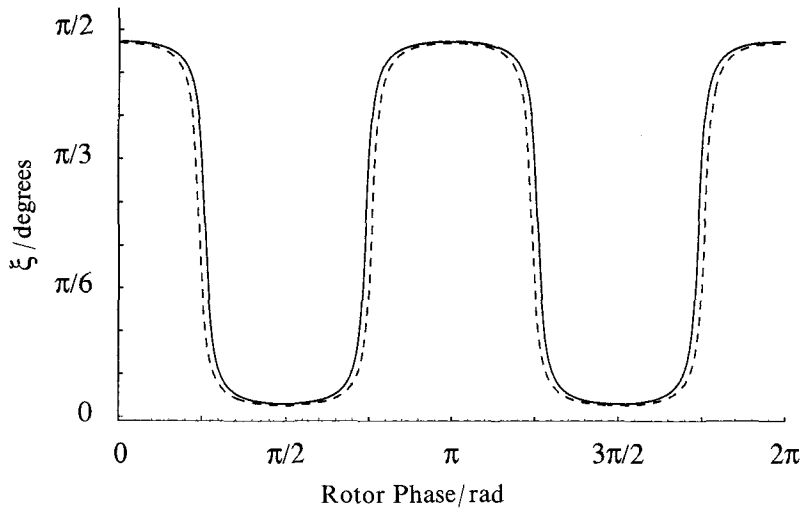

Figure 1. Plots of ξ_1 (— — —) and ξ_2 (———) as functions of rotor phase for a crystallite spinning about the magic angle (54·74°) with PAS oriented perpendicular to the rotor, $\epsilon^2 qQ/h = 11{\cdot}0$ MHz and $\eta = 0{\cdot}0$.

In figure 1 is a plot of the values of ξ_1 and ξ_2 for a typical crystallite as a function of the rotor phase for a complete rotation. Note that, for a majority of the rotor period, both ξ_1 and ξ_2 have values near either 0 or $\frac{1}{2}\pi$. Therefore, for the majority of the rotor period, the Hamiltonian in equation (8) can be written in terms of single and triple quantum operators as either

$$\tilde{H}(\xi \approx 0) \approx -\omega_{1I} I_z - 2\omega_{1S} S_z^{2-3} + \omega_Q (S_{00}^{1-4} - S_{00}^{2-3}) - 6\omega_D A_{20}^D(t) I_x S_x^{1-4} + 2\omega_D A_{20}^D(t) I_x S_x^{2-3} \tag{23}$$

or

$$\tilde{H}(\xi \approx \tfrac{1}{2}\pi) \approx -\omega_{1I} I_z + 2\omega_{1S} S_z^{1-4} - \omega_Q (S_{00}^{1-4} - S_{00}^{2-3}) - 2\omega_D A_{20}^D(t) I_x S_x^{1-4} + 6\omega_D A_{20}^D(t) I_x S_x^{2-3}. \tag{24}$$

In general, the time-ordering operator T makes the integral in equation (12) complicated since $\tilde{H}(t)$ and $\dot{W}^\dagger(t) W(t)$ do not commute with each other at all times. There are, however, certain approximations that can simplify this task. The adiabatic approximation is permitted when $|\tilde{H}(t)| \gg |\dot{W}^\dagger(t) W(t)|$, and the sudden approximation is permitted when $|\tilde{H}(t)| \ll |\dot{W}^\dagger(t) W(t)|$.

If the adiabatic approximation holds when $A_{20}^Q(t)$ passes through the extremum in $\dot{W}^\dagger(t) W(t)$, the level crossing is avoided and the propagator for all times can be written

$$\tilde{U}_a(t) = \exp\left(-i \int_0^t \tilde{H}(s)\, ds\right). \tag{25}$$

Under the Hartmann–Hahn matching condition $\omega_{1I} = (S + \frac{1}{2})\omega_{1S}$, and assuming that we start with a crystallite where $\xi_1 \approx \xi_2 \approx 0$, adiabatic evolution of I_z under the Hamiltonian of equation (23) leads to

$$\tilde{U}_a(t) I_z \tilde{U}_a^\dagger(t) \rightarrow \tfrac{1}{2}(I_z + S_z^{2-3}), \tag{26}$$

and polarization is transferred from the I spin to the central transition of the S spin. CP transfer is interrupted while the sample rotation takes the first-order quadrupolar coupling through zero. After the zero crossing, ξ_1 and ξ_2 take on values near $\frac{1}{2}\pi$, and adiabatic evolution of I_z under the Hamiltonian of equation (24) leads to

$$\tilde{U}_a(t) I_z \tilde{U}_a^\dagger(t) \rightarrow \tfrac{1}{2}(I_z + S_z^{1-4}). \tag{27}$$

During MAS, this process occurs twice or four times every rotor period depending on the PAS orientation. In addition, S_z^{2-3} and S_z^{1-4} remain spin locked and unchanged during those periods when they are not involved in polarization transfer. While the polarization transfer from I_z is switching between S_z^{2-3} and S_z^{1-4}, the effective observable is also approximated as switching between

$$\tilde{S}_+(\xi \approx 0) \approx 2S_z^{2-3} - 3^{1/2}(S_x^{1-3} + S_x^{2-4}) + 3^{1/2}\mathrm{i}(S_y^{1-2} + \tfrac{2}{3^{1/2}} S_y^{2-3} + S_y^{3-4}) \tag{28}$$

and

$$\tilde{S}_+(\xi \approx \tfrac{1}{2}\pi) \approx -2S_z^{1-4} + 3^{1/2}(S_z^{1-3} - S_x^{2-4}) + 3^{1/2}\mathrm{i}(S_y^{1-2} + \tfrac{2}{3^{1/2}} S_y^{1-4} + S_y^{3-4}) \tag{29}$$

respectively. As shown by Vega [12], after multiple zero crossings the central and triple quantum transitions will be equally polarized from the I spin. The overall CP intensity will be identical with that observed for a static spin in the thermodynamic limit. However, the overall rate will be half as fast, since both the central and the triple quantum transitions are being polarized simultaneously. In the presence of a short rotating frame relaxation time, this will lead to a reduced overall CP intensity from the spins undergoing adiabatic zero crossings.

When the sudden approximation holds, the propagator can be written

$$\tilde{U}_s(t) = \exp\left(\int_0^t \dot{W}^\dagger(s) W(s)\, \mathrm{d}s\right). \tag{30}$$

While this propagator does not hold for all times, the term $\dot{W}^\dagger(t) W(t)$ has the form of an impulse function with an integrated area of $\frac{1}{2}\pi$ centred near the zero crossing of $A_{20}^{Q}(t)$. This results in a discontinuous transition between the adiabatic propagator of equation (25) and the sudden propagator of equation (30) (figure 2). Under the sudden propagator, S_z^{2-3} and S_z^{1-4} transform according to

$$\tilde{U}_s(t) S_z^{2-3} \tilde{U}_s^\dagger(t) \rightarrow S_z^{1-4} \tag{31}$$

and

$$\tilde{U}_s(t) S_z^{1-4} \tilde{U}_s^\dagger(t) \rightarrow S_z^{2-3}. \tag{32}$$

Therefore this coefficients of the S_z^{2-3} and S_z^{1-4} terms in the density matrix will be exchanged after evolving through a sudden zero crossing. After multiple zero crossings, one of the two transitions will be completely polarized while the other will be unpolarized. The observable operator will always match the cross polarizing transition; so the polarized intensity will always remain observable, and the CP efficiency and rate should be identical with the static case.

Crystallites which pass through the zero crossing in neither an adiabatic nor a sudden regime fall into the intermediate regime. This type of evolution is the most difficult to calculate analytically. To determine the evolution of the density matrix in

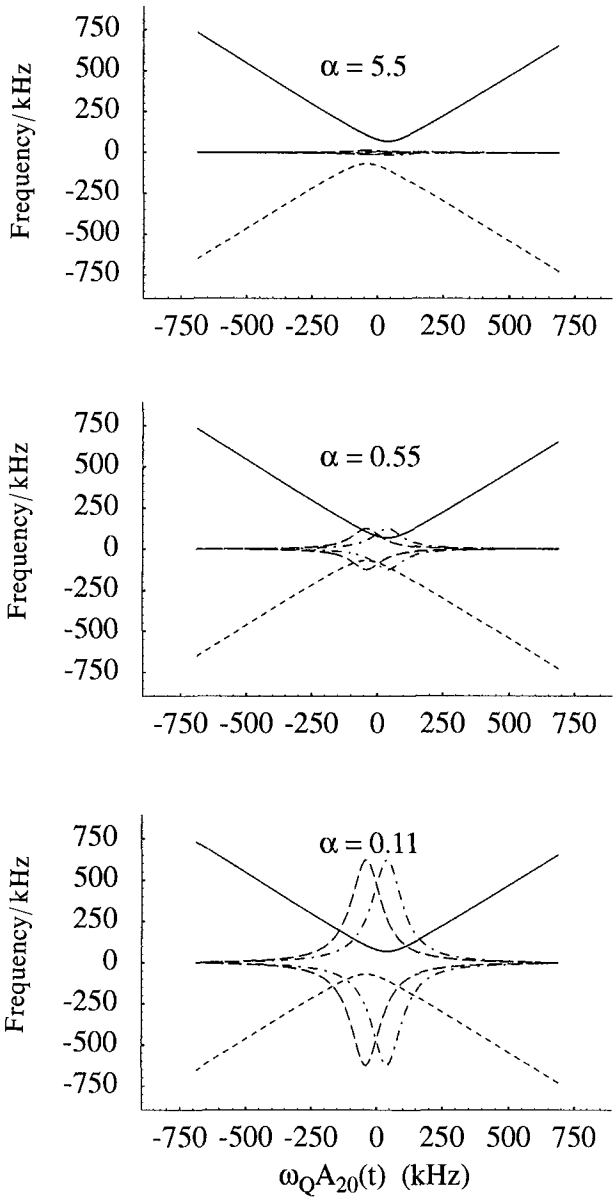

Figure 2. Plot of diagonal and off-diagonal coefficients ω^{1-3} (——), ω^{2-4} (- - - -), $d(2\xi_1)/dt$ (– · –) and $d(2\xi_2)/dt$, (— — —) of the time-dependent frame Hamiltonian in equations (13) and (20), as functions of $\omega_Q A_{20}^Q(t)$. The off-diagonal coefficients have the form of Lorenztian impulse functions as follows:

$$\frac{d[2\xi_1(t)]}{dt} = \frac{3^{1/2}\omega_{1S}\omega_Q}{[-\omega_Q A_{20}^Q(t) + \omega_{1S}]^2 + 3\omega_{1S}^2} \frac{dA_{20}^Q(t)}{dt}$$

and

$$\frac{d[2\xi_2(t)]}{dt} = \frac{3^{1/2}\omega_{1S}\omega_Q}{[\omega_Q A_{20}^Q(t) + \omega_{1S}]^2 + 3\omega_{1S}^2} \frac{dA_{20}^Q(t)}{dt}.$$

the intermediate regime, contributions from both $\tilde{H}(t)$ and $\dot{W}^{\dagger}(t)W(t)$, which do not commute at all times, must be used to construct the propagator. Vega [11, 12] has shown with numerical simulations that spins undergoing an intermediate-regime zero crossing evolve into non-spin-locked states and thus result in a significant loss of CP intensity. To indicate whether a zero crossing is in the adiabatic, intermediate or sudden regime, an adiabaticity parameter α is defined:

$$\alpha = \frac{\omega^{1-3}(t_0^{1-3})}{\{\mathrm{d}[2\xi_1(t)]/\mathrm{d}t\}|_{t_0^{1-3}}} = -\frac{\omega^{2-4}(t_0^{2-4})}{\{\mathrm{d}[2\xi_2(t)]/\mathrm{d}t\}|_{t_0^{2-4}}} = \frac{3\omega_{1S}^2}{\omega_Q}\frac{\mathrm{d}t}{\mathrm{d}A_{20}^{Q}(t)}\bigg|_{t_0^{1-3}}. \tag{33}$$

This is then evaluated at either of the zero crossings, $\omega_Q A_{20}^{Q}(t_0^{1-3}) \approx \omega_{1S}$ or $\omega_Q A_{20}^{Q}(t_0^{2-4}) \approx -\omega_{1S}$, corresponding to a maximum in the $\dot{W}^{\dagger}(t)W(t)$ term when ξ_1 or ξ_2 goes through $\frac{1}{4}\pi$. This definition of the adiabaticity parameter is proportional to that used by Vega; however, now there is an additional orientation dependence as well which comes from the time derivative of $A_{20}^{Q}(t)$. When the value of α at the zero crossing is much larger than, much less than, or of the order of one, the crossing will be adiabatic, sudden or intermediate respectively.

In a multisite system it may be difficult or even impossible to adjust α (by changing the spinning rate or r.f. power levels) for optimal CP transfer of all sites while spinning at the magic angle. One solution that eliminates the problem is to exploit the time independence of the spin eigenvalues when spinning at 0° (parallel) to the external magnetic field direction. By performing CP while spinning at 0°, none of the spins undergoes zero crossing and the full static CP intensity can be recovered. We call this approach ZPMAS and ZPVAS for zero-polarized MAS and VAS, respectively. In the next section, we show experimental examples using these approaches.

The theory for the DAS experiment has been described previously [13, 14, 24, 25]. In the DAS experiment, there exists a continuous distribution of angle pairs with the basic requirements that the evolution periods $t_1/(k+1)$ at the first angle θ_1 and $kt_1/(k+1)$ at the second angle θ_2 fulfil the following pair of equations:

$$\begin{aligned} P_2(\cos\theta_1) &= -kP_2(\cos\theta_2), \\ P_4(\cos\theta_1) &= -kP_4(\cos\theta_2), \end{aligned} \tag{34}$$

where $P_n(x)$ is the nth order Legendre polynomial of x.

3. Results and discussion

The effect of level crossings on CP efficiency can be seen clearly in figure 3, which shows the CP efficiencies of sodium hydroxide ($NaOH \cdot xH_2O$), and sodium pyruvate ($CH_3OCOONa$) against VAS angle. All intensities are scaled relative to the corresponding single-pulse ^{23}Na VAS and MAS spectra, using the sequence given later in

Figure 2. *Continued.*
The crystallite parameters are identical with those in figure 1. The curves in (*a*) are for a spinning rate of 100 Hz which has an adiabaticity parameter α of 5·5. The curves in (*b*) are for a spinning rate of 1 kHz which has an adiabacity parameter α of 0·55. The curves in (*c*) are for a spinning rate of 5 kHz which has an adiabaticity parameter α of 0·11 (sudden regime).

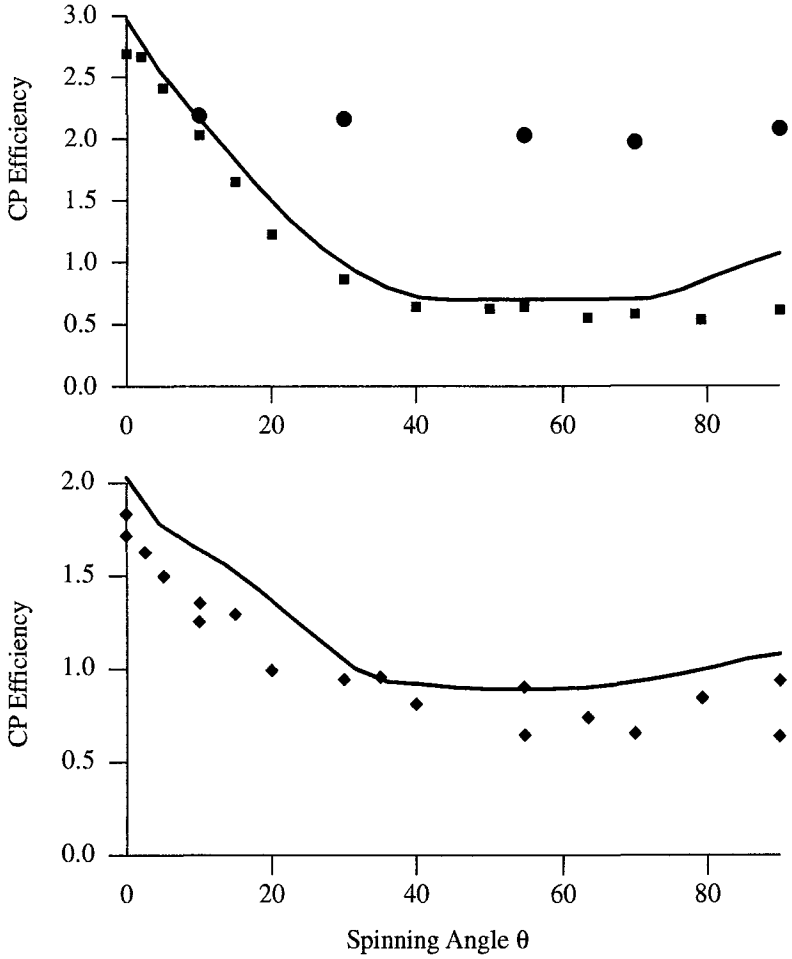

Figure 3. CP intensity as a function of VAS angle for sodium pyruvate (■) and sodium hydroxide (◆). The results for sodium pyruvate using the ZPVAS experiment (●) are also shown. Curves through points are arrived at numerically as discussed in the text.

figure 7. As expected, only under static (0° VAS) conditions do we achieve the expected CP efficiency maximum of approximately $\gamma_1/2\gamma_2$ for sodium hydroxide and $3\gamma_1/4\gamma_2$ for sodium pyruvate. The factors of $\frac{1}{2}$ and $\frac{3}{4}$ are due to the high abundance of both ^{1}H and ^{23}Na, causing CP to be controlled by the equilibrium between their respective spin temperatures. As the VAS angle increases, CP efficiency decreases dramatically. Spinning the sample at an angle greater than approximately 25° results in an efficiency that is less than that achieved by a single pulse. This indicates that the level crossings are significant, even when only a reduced fraction of the spins are undergoing the maximum four crossings per rotor cycle.

We can calculate the approximate CP efficiency at any given spinning angle (the curves in figure 3) by first determining the number of crystallites with ξ_1 and ξ_2 excursions within $\frac{1}{12}\pi$ of 0 or $\frac{1}{2}\pi$ and thus capable of Hartmann–Hahn matching. Secondly, of those spins which can cross polarize, we sum the number that undergo adiabatic or sudden zero crossings. The adiabatic spins are assigned an arbitrary intensity between 0·5 and 1·0 since they may not be fully cross polarized before

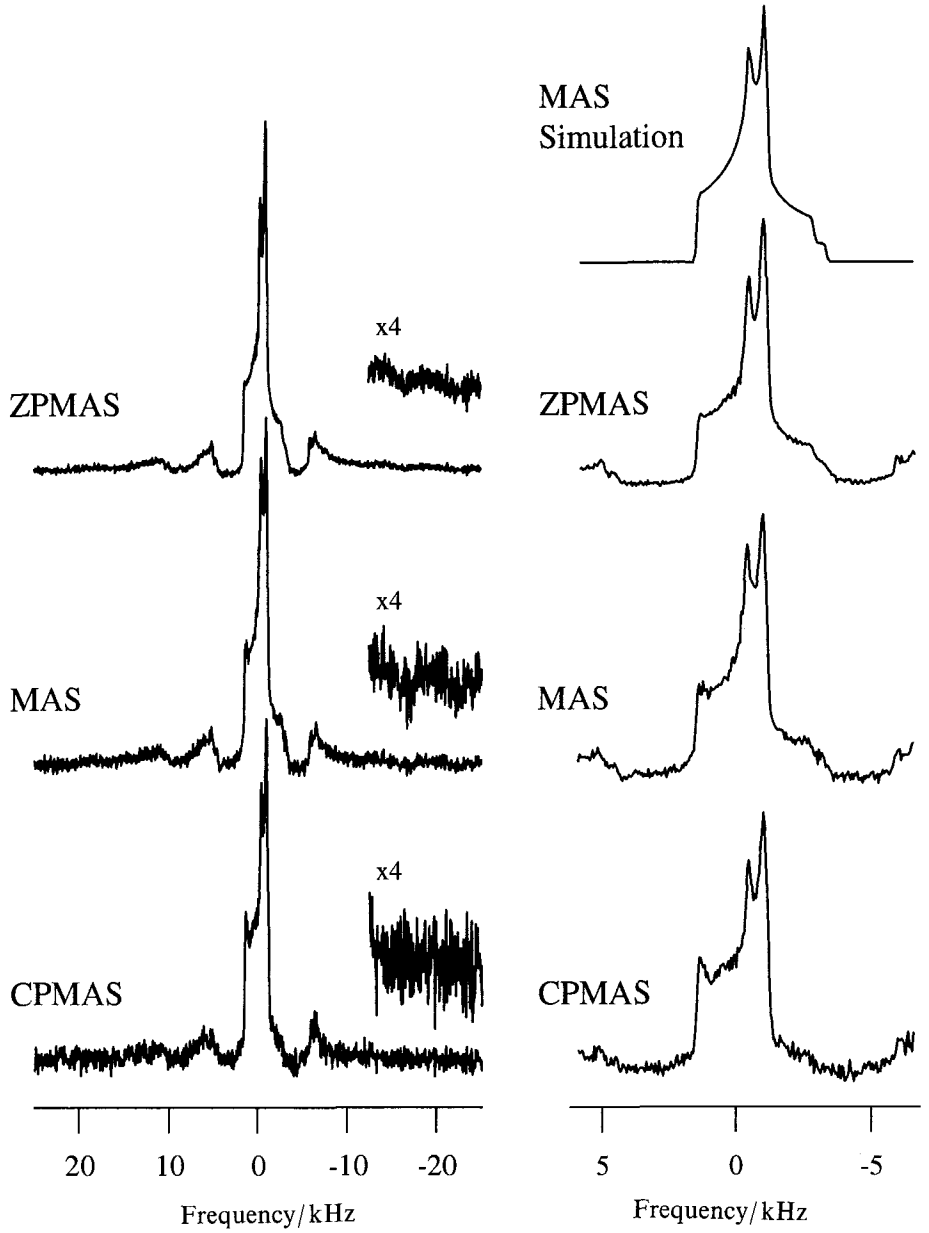

Figure 4. MAS spectra of sodium pyruvate acquired with MAS, CPMAS and ZPMAS pulse sequences. Spectra on the right are expanded to show the centre band more clearly. The insets show magnified sections of the baseline for better comparison of signal-to-noise ratios.

rotating frame relaxation begins to impede the CP build-up while the sudden spins are assigned an intensity of 1·0. For sodium hydroxide and sodium pyruvate, the values of e^2qQ/h were 1·8 and 2·36 MHz and η were 0·0 and 0·77 respectively in these calculations. The parameters for sodium pyruvate were obtained from simulations of the MAS spectrum while those of sodium hydroxide were taken from Vega [12].

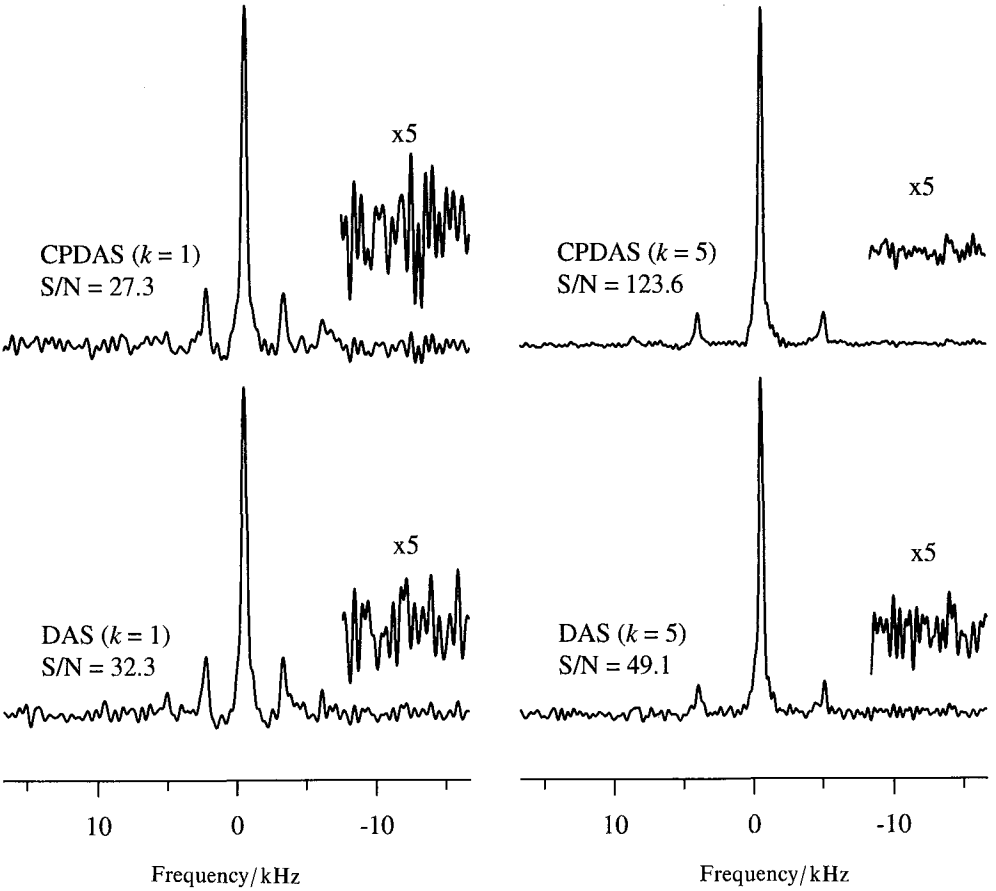

Figure 5. DAS spectra of sodium pyruvate acquired at both $k = 1$ and $k = 5$ with both DAS and CPDAS pulse sequences. Insets show magnified sections of the baseline for better comparison of signal-to-noise ratios S/N.

Figure 3 also shows the CP efficiency for sodium pyruvate at the angle at which detection occurred under ZPVAS. Since CP always occurs at 0°, the observed efficiency is constant for all angles. However, the efficiency under ZPVAS is less than that observed under 0° VAS because of T_1 relaxation processes that occur during the hop from 0° to the detection angle.

In figure 4, we show the ^{1}H-decoupled MAS spectra of sodium pyruvate acquired with and without CP and with ZPMAS together with the simulation of the MAS powder pattern. The signal-to-noise ratio is the worst for CPMAS, about 75% of that seen in the MAS spectrum without CP. On the other hand, the ZPMAS spectrum has a signal-to-noise ratio about twice that seen in the MAS spectrum taken without CP.

In figure 5, the decoupled DAS and CPDAS spectra of sodium pyruvate for the 0°–63·43° ($k = 5$) and 37·38°–79·19° ($k = 1$) angle pairs are compared. For $k = 5$, we observe over 2·5 times the signal-to-noise ratio in the spectrum taken with CP compared with the spectrum taken without CP. In addition, the CPDAS experiment at $k = 5$ has a signal-to-noise ratio over 4·5 times that of the CPDAS experiment at $k = 1$. This demonstrates the importance of 0° CP for DAS. The CPDAS experiment

done at 37·38° ($k = 1$) has a worse signal-to-noise ratio than the same experiment done without CP. Other k values will also have reduced CP efficiencies, in addition to having spinning side-band patterns which are more complicated than in the $k = 1$ or 5 cases [25].

4. Dynamic-angle spinning dipolar linewidth

While DAS removes second-order anisotropic broadenings it fails to remove first-order homonuclear dipolar broadenings. This is because the $\frac{1}{2}\pi$ pulses applied before and after changing angles fail to store all density matrix elements owing to homonuclear spin–spin interactions. This results in a dipolar dephasing that is not refocused while spinning at the second DAS angle. However, since DAS utilizes a continuous set of complementary angle pairs, the degree of dipolar dephasing depends on the choice of the DAS angle pair.

Using an approximation which describes the dipolar dephasing of a static homonuclear bath of spins as a Gaussian decay, the signal for an on-resonance spin may be written as

$$S(t) = \exp(-\tfrac{1}{2}M_2 t^2), \tag{35}$$

where M_2 is the second moment as defined by Van Vleck [26]. Under fast spinning conditions ($\omega_r > \omega_D$), the effective dipolar coupling is scaled by $P_2(\cos\theta)$ and therefore the effective second moment is $M_2 P_2^2(\cos\theta)$ (remember that θ is the rotation axis orientation with respect to the magnetic field). The signal for an on-resonance spin undergoing fast VAS is

$$S(t) = \exp[-\tfrac{1}{2}M_2 P_2^2(\cos\theta)t^2]. \tag{36}$$

In a DAS experiment, the sample evolves under fast VAS conditions at two different angles. Therefore, the signal for an on-resonance spin will be

$$\begin{aligned} S(t_1) &= \exp\left[-\tfrac{1}{2}M_2 P_2^2(\cos\theta_1)\left(\frac{t_1}{k+1}\right)^2\right] \exp\left[-\tfrac{1}{2}M_2 P_2^2(\cos\theta_2)\left(\frac{kt_1}{k+1}\right)^2\right] \\ &= \exp(-\tfrac{1}{2}M_2^{\text{eff}} t_1^2) \end{aligned} \tag{37}$$

For the DAS angle pairs θ_1 and θ_2, the value of $P_2(\cos\theta)$ can be expressed in terms of k (from equation (34)) where $P_2(\cos\theta_1) = (\frac{1}{5}k)^{1/2}$ and $P_2(\cos\theta_2) = -(\frac{1}{5}k)^{1/2}$. This equation yields an effective second moment for the isotropic line in the DAS experiment of $M_2^{\text{eff}} = 2kM_2/5(k+1)^2$, giving a linewidth

$$\Delta\omega \approx \frac{(2kM_2)^{1/2}}{5^{1/2}(k+1)}. \tag{38}$$

The narrowest line in a conventional DAS experiment should therefore arise when the $k = 5$ angle pair 0°–63·43° is used and should be about 75% of the linewidth for a $k = 1$ experiment.

The dipolar linewidths for sodium oxalate ($Na_2C_2O_4$), rubidium perchlorate ($RbClO_4$) and deuterated boric acid (D_3BO_3) are shown in figure 6 for a range of k values from 0·8 to 5. It is always true that the linewidth at $k = 5$ is about 20% less than at $k = 1$ in agreement with equation (38). The solid curves through these data points are the best fitted using the function

$$\Delta\omega_{\text{isotropic}} = \Delta\omega_{T_2} + \frac{(2kM_2)^{1/2}}{5^{1/2}(k+1)}, \tag{39}$$

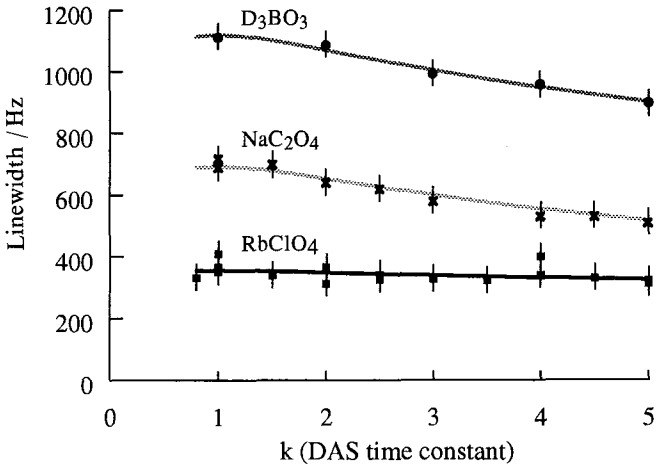

Figure 6. Isotropic linewidth of boric acid (top), sodium oxalate (bottom) and rubidium perchlorate. The curves are the best fits from equation (39).

where M_2 is the second moment due to homonuclear dipole interactions in a static sample and $\Delta\omega_{T_2}$ is the intrinsic linewidth due to field inhomogeneity and T_2 relaxation. The values for M_2 extracted in this manner are very similar to those extracted from static Carr–Purcell–Meiboom–Gill (CPMG) experiments. This further confirms that the $k = 5$ angle pair is the best angle pair with which to perform the DAS experiment.

5. Experimental details

The CP experiments were performed on a home-built spectrometer at 7·04 T (^{1}H NMR frequency of 301·200 MHz and ^{23}Na frequency of 79·671 MHz). The DAS probe was home built with a stationary coil of 0·75 in diameter for both r.f. transmission and detection [27]. The double-tuned r.f. resonant circuit was similar to that described by Doty *et al.* [28, 29]. The input power of 300 W on the ^{1}H channel and 100 W on the ^{23}Na channel gave 7 μs central transition selective $\frac{1}{2}\pi$ rotations and the spinning rate was between 4·0 and 6·6 kHz. The samples of sodium hydroxide and sodium pyruvate used for these experiments were obtained from standard commer-

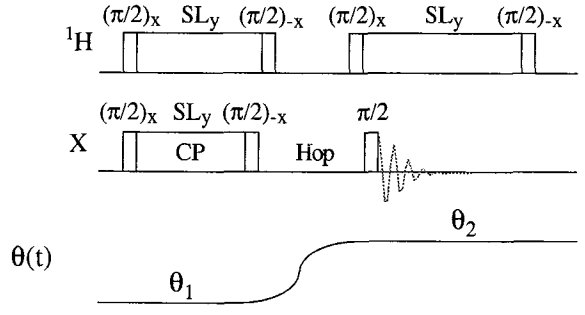

Figure 7. One-dimensional ZPVAS pulse sequence. The axis angle with respect to time is shown below the sequence. SL refers to spin lock. Subscripts refer to the phases of pulses.

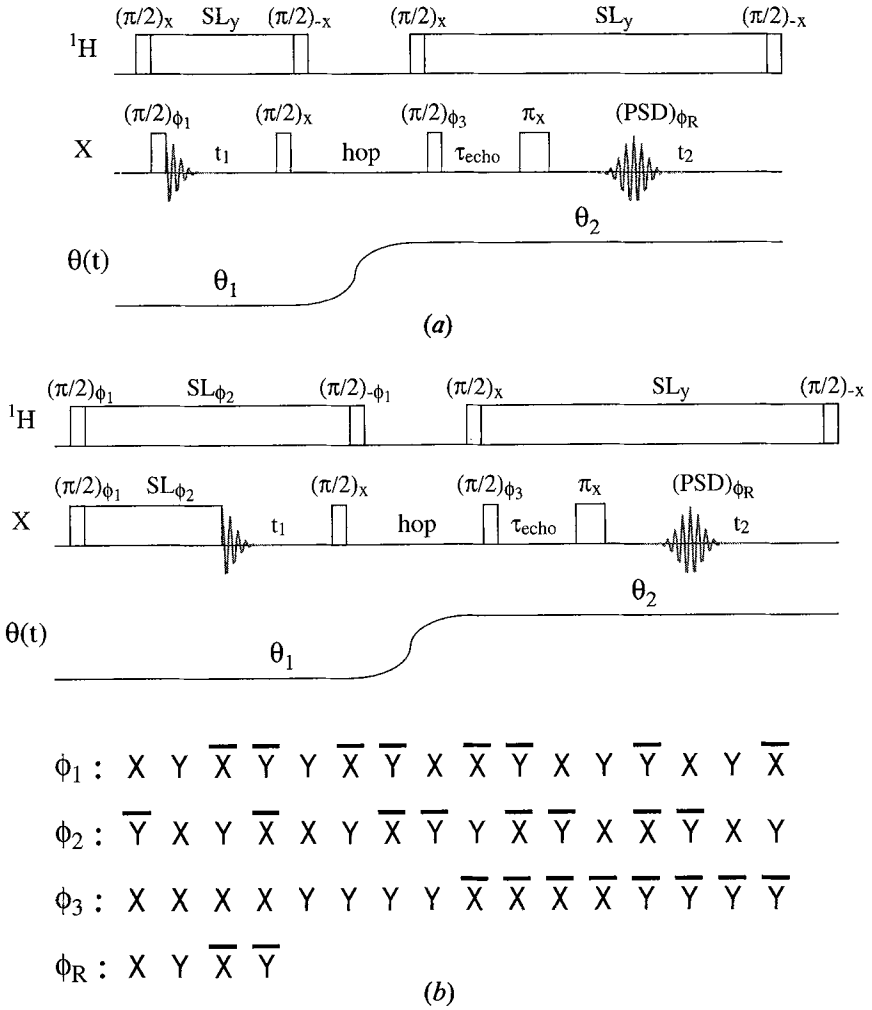

Figure 8. (*a*) Pulse sequence for two-dimensional ^{1}H-decoupled DAS. The r.f. pulse phase cycle is given in [24]. (*b*) Pulse sequence and r.f. pulse phase cycle for two-dimensional ^{1}H-decoupled CPDAS pulse sequences. Details of the data treatment required with these sequences has been described in [24]. In both figures, SL refers to spin lock, PSD refers to phase-sensitive detection, subscripts refer to pulse phases, and $\theta(t)$ refers to the axis orientation.

cial sources. The pulse sequence for ZPVAS is given in figure 7, and the pulse sequence for CPDAS is given in figure 8. For the CP efficiency experiments, phase alternation of the ^{1}H r.f. was used to assure that only the intensity due to CP could be measured. Additional details on the DAS pulse sequence and data processing have been described previously [24]. For CPDAS and ZPVAS experiments, a $\frac{1}{2}\pi$ pulse was applied on the ^{23}Na simultaneously with the initial ^{1}H $\frac{1}{2}\pi$ to achieve the largest final sodium polarization. For the ^{23}Na spectra without CP, recycle delays of 30 s and 16 s were used for the sodium hydroxide and sodium pyruvate respectively while for the CP experiments recycle delays of 10 min and 36 s respectively were used to assure complete relaxation for accurate intensity comparisons. For the DAS

experiments we acquired 32 scans for each of the 90 t_1 points while for the CP build-up curves and ZPVAS spectra we acquired four, eight or 64 scans for each different contact time and angle pair respectively. For the CPDAS and ZPVAS experiments on sodium pyruvate the CP contact time was 20 ms. The contact time for sodium hydroxide was 2 ms.

For the isotropic linewidth measurements, samples of sodium oxalate and rubidium perchlorate were obtained from commercial sources while the deuterated boric acid was made by exchanging the protons in boric acid (H_3BO_3) with deuterium oxide (D_2O), both commercially obtained. The experiments were performed at 11·7 T (^{87}Rb frequency, 163·623 MHz; ^{23}Na frequency, 132·201 MHz; ^{11}B frequency, 160·446MHz) with the same probe as above. The pulse sequence used for DAS was the same as above although without decoupling. The selective $\frac{1}{2}\pi$ times were between 4 and 8 μs and the recycle delays were between 1 and 4 s. The spinning speeds were between 5·0 and 7·0 kHz which effectively removed all spinning side-bands from these spectra. The sweep widths were set to 10 kHz, and between 256 and 1024 scans were acquired for each of 60 t_1 points at each k value.

6. Conclusion

We have shown that the efficiency of CP can be strongly attenuated unless the spinning axis is close to 0°. Therefore in any VAS or DAS experiment it will be difficult to achieve maximum CP efficiency unless one does the magnetization transfer at 0° as a part or before starting the experiment. In addition, for the case of DAS, the choice of 0° and 63·43° possess the additional benefit of giving the largest effective spinning speed, $\frac{5}{6}\omega_r$, and narrowest residual homonuclear dipolar linewidth. These results should prove quite valuable for systems with low abundance such as ^{87}Rb (27·8% abundant) or where isotopic labelling is crucial such as ^{17}O (0·037% abundant), which could have polarization enhancements of 3·1 and 7·4 respectively, leading to large savings in experiment time. In addition, for spin-$\frac{1}{2}$ systems (such as ^{1}H–^{13}C or ^{1}H–^{15}N), where the time modulation of the dipolar interaction leads to modulations of the Hartmann–Hahn match condition, the use of ZPMAS may yield better CP efficiencies and reduce CPMAS distortions.

We wish to thank Lyndon Emsley and Lucio Frydman for helpful discussions. This investigation was supported by the Director, Office of Energy Research, Office of Basic Energy Sciences, Materials Sciences Division, US Department of Energy, under Contract No. DE-AC03-76SF00098. J. H. B. was supported by a National Science Foundation graduate fellowship.

Appendix 1. Fictitious spin-$\frac{1}{2}$ formalism

$$S_x^{r-s} = \tfrac{1}{2}(|r\rangle\langle s| + |s\rangle\langle r|),$$
$$S_y^{r-s} = \tfrac{1}{2}\mathrm{i}(-|r\rangle\langle s| + |s\rangle\langle r|),$$
$$S_z^{r-s} = \tfrac{1}{2}(|r\rangle\langle r| - |s\rangle\langle s|),$$
$$S_{00}^{r-s} = \tfrac{1}{2}(|r\rangle\langle r| + |s\rangle\langle s|),$$

$$\exp(-i\xi S_x^{r-s}) \begin{Bmatrix} S_x^{s-t} \\ S_y^{s-t} \\ S_z^{s-t} \\ S_{00}^{s-t} \end{Bmatrix} \exp(i\xi S_x^{r-s}) = \begin{cases} S_x^{s-t} \cos(\frac{1}{2}\xi) + S_y^{r-t} \sin(\frac{1}{2}\xi), \\ S_y^{s-t} \cos(\frac{1}{2}\xi) - S_x^{r-t} \sin(\frac{1}{2}\xi), \\ S_z^{s-t} \cos^2(\frac{1}{2}\xi) + S_z^{r-t} \sin^2(\frac{1}{2}\xi) + \frac{1}{2} S_y^{r-s} \sin\xi, \\ S_{00}^{s-t} \cos^2(\frac{1}{2}\xi) + S_{00}^{r-t} \sin^2(\frac{1}{2}\xi) + \frac{1}{2} S_y^{r-s} \sin\xi, \end{cases}$$

$$\exp(-i\xi S_y^{r-s}) \begin{Bmatrix} S_x^{s-t} \\ S_y^{s-t} \\ S_z^{s-t} \\ S_{00}^{s-t} \end{Bmatrix} \exp(i\xi S_y^{r-s}) = \begin{cases} S_x^{s-t} \cos(\frac{1}{2}\xi) - S_y^{r-t} \sin(\frac{1}{2}\xi), \\ S_y^{s-t} \cos(\frac{1}{2}\xi) - S_y^{r-t} \sin(\frac{1}{2}\xi), \\ S_z^{s-t} \cos^2(\frac{1}{2}\xi) + S_z^{r-t} \sin^2(\frac{1}{2}\xi) - \frac{1}{2} S_x^{r-s} \sin\xi, \\ S_{00}^{s-t} \cos^2(\frac{1}{2}\xi) + S_{00}^{r-t} \sin^2(\frac{1}{2}\xi) - \frac{1}{2} S_x^{r-s} \sin\xi, \end{cases}$$

$$\exp(-i\xi S_z^{r-s}) \begin{Bmatrix} S_x^{s-t} \\ S_y^{s-t} \\ S_z^{s-t} \\ S_+^{s-t} \\ S_-^{s-t} \end{Bmatrix} \exp(i\xi S_z^{t-s}) = \begin{cases} S_x^{s-t} \cos(\frac{1}{2}\xi) - S_x^{s-t} \sin(\frac{1}{2}\xi), \\ S_y^{s-t} \cos(\frac{1}{2}\xi) + S_x^{s-t} \sin(\frac{1}{2}\xi), \\ S_z^{s-t}, \\ S_+^{s-t} \exp(\frac{1}{2}i\xi), \\ S_-^{s-t} \exp(\frac{1}{2}i\xi), \end{cases}$$

References

[1] Pines, A., Gibby, M. G., and Waugh, J. S., 1973, *J. chem. Phys.*, **59,** 569.
[2] Alla, M., and Lippmaa, E., 1976, *Chem. Phys. Lett.*, **37,** 260.
[3] Rybaczewisky, E. F., Neff, B. L., Waugh, J. S., and Sherfinski, J. S., 1977, *J. chem. Phys.*, **67,** 1231.
[4] Webb, G. G. and Zilm, K. W., 1989, *J. Am. chem. Soc.*, **111,** 1455.
[5] VanderHart, D. L., and Campbell, G. C., 1990, *31st Experimental Nuclear Magnetic Resonance Conference*, Asilomar, CA (unpublished).
[6] Sethi, N. K., 1991, *J. Magn. Reson.*, **94,** 352.
[7] Burum, D. P., and Bielecki, A., 1991, *J. magn. Reson.*, **95,** 184.
[8] Fyfe, C. A., Grondey, H., Mueller, K. T., Wong-Moon, K. C., and Markus, T., 1992, *J. Am. chem. Soc.*, **114,** 5876.
[9] Wu, X., and Zilm, K. W., 1993, *J. magn. Reson.* A, **102,** 205.
[10] Stejskal, E. O., Schaefer, J., and Waugh, J. S., 1977, *J. magn. Reson.*, **28,** 105.
[11] Vega, A. J., 1992, *J. magn. Reson.*, **96,** 50.
[12] Vega, A. J., 1992, *Solid St. NMR*, **1,** 17.
[13] Llor, A., and Virlet, J., 1988, *Chem. Phys. Lett.*, **152,** 248.
[14] Mueller, K. T., Sun, B. Q., Chingas, G. C., Zwanziger, J. W., Terao, T., and Pines, A., 1990, *J. magn. Reson.*, **86,** 470.
[15] Samoson, A., Sun, B. Q., and Pines, A., 1992, *New Angles in Motional Averaging*, edited by D. M. S. Bagguley (Clarendon).
[16] Grandinetti, P. J., Lee, Y. K., Baltisberger, J. H., Llor, A., and Pines, A., 1992, *34th Rocky Mountain Conference on Analytical Chemistry*, Denver, CO.
[17] Gann, S. L., Baltisberger, J. H., Grandinetti, P. J., Wooten, E. W., and Pines, A., 1993, *34th Experimental Nuclear Magnetic Resonance Conference*, St. Louis, MO.
[18] Gann, S. L., Baltisberger, J. H., Wooten, E. W., Zimmermann, H., and Pines, A., 1994, *Bull. magn. Reson.*, **16,** 68.
[19] Fyfe, C. A., Mueller, K. T., Grondey, H., and Wong-Moon, K. C., 1993, *34th Experimental Nuclear Magnetic Resonance Conference*, St. Louis, MO.
[20] Fyfe, C. A., Wong-Moon, K. C., Grondey, H., and Mueller, K. T., *J. Phys. Chem.* (submitted).
[21] Wokaun, A., and Ernst, R. R., 1977, *J. chem. Phys.*, **67,** 1752.
[22] Vega, S., 1978, *J. chem. Phys.*, **68,** 5518.

[23] VEGA, S., and NAOR, Y., 1981, *J. chem. Phys.*, **75,** 75.
[24] GRANDINETTI, P. J., BALTISBERGER, J. H., LLOR, A., LEE, Y. K., WERNER, U., EASTMAN, M. A., and PINES, A., 1993, *J. magn. Reson.* A, **103,** 72.
[25] GRANDINETTI, P. J., LEE, Y. K., BALTISBERGER, J. H., SUN, B. Q., and PINES, A., 1993, *J. magn. Reson.* A, **102,** 195.
[26] VAN VLECK, J. H., 1948, *Phys. Rev.*, **74,** 1168.
[27] MUELLER, K. T., CHINGAS, G. C., and PINES, A., 1991, *Rev. scient. Instrum.*, **62,** 1445.
[28] DOTY, F. D., INNERS, R. R., and ELLIS, P. D., 1981, *J. magn. Reson.*, **43,** 399.
[29] DOTY, F. D., CONNICK, T. J., NI, X. Z., and CLINGAN, M. N., 1988, *J. magn. Reson.*, **77,** 536.